Quantitative assessment of structural components for construction management using laser scanning data

Truong-Hong, Linh; Lindenbergh, R.C.

Publication date
2020

Document Version
Final published version

Published in
Proceedings of the FIG Working Week 2020

Citation (APA)
Truong-Hong, L., & Lindenbergh, R. C. (2020). Quantitative assessment of structural components for construction management using laser scanning data. In *Proceedings of the FIG Working Week 2020: Smart Surveyors for Land and Water Management* International Federation of Surveyors (FIG).

Quantitative Assessment of Structural Components for Construction Management Using Laser Scanning Data

Linh TRUONG-HONG and Roderik LINDENBERGH, Netherlands

Key words: Point Cloud, Structural Component Extraction, Segmentation, Deformation, Surface Defects, Inspection

SUMMARY

Defects in a construction site is inevitable and these defects must be inspected and reported timely to minimize extract cost due to repair the defects. However, in practice, quality of structural elements is often inspected by a site supervisor with traditional tools (e.g. measuring tapes, total stations or levelling) at only specific locations on the structures. That results the current inspection pipeline is subjective and inefficient. As such, a new approach must develop to support project managers reporting surface defects timely and using a digital tool in project management efficiently. A great achievement of laser scanning platforms allows to acquire three-dimensional (3D) topographic data of structures' surfaces in a construction site quickly and accurately. A current terrestrial laser scanner (TLS) can capture more than a million points per second with a sub-millimetre accuracy. This technology has been gradually implemented in evaluating progress, quality and quantity, and visualisation for construction management. However, a processing point cloud requires intensive labour work because of the complexity of the construction site and massive data points. This paper is to develop the algorithm to automatically access structural components for quality control of the construction project, in which the proposed method is focused to evaluate the flatness of the floors and ceiling. The method starts to decompose the point cloud of the building storey into 2D cells by using a quadtree. Subsequently, a combination of kernel density estimation (KDE) and cell-based segmentation (CbS) to extract the data point affiliated surfaces of the floor and ceiling. Next, edges of the slabs are detected and then are used to generate the reference surface to compute deformations by using both point- and cell-surface methods. The proposed method is tested on 23.9-million-point cloud of a storey of the reinforced concrete building acquired from the TLS. An experimental test shows the proposed method successfully extracts all surfaces of the floors and ceiling and a report also shows the slab deformation varying in a range from -36.04mm to 42.03mm for point-surface method and about 75% of the deformation is within a range of mean ± standard deviation.

Quantitative Assessment of Structural Components for Construction Management Using Laser Scanning Data

Linh TRUONG-HONG and Roderik LINDENBERGH, Netherlands

1. INTRODUCTION

In construction projects, defects of structural components are inevitable, which can cost about 10.29% of the complete costs in civil infrastructure projects (Love Peter, 2002). To minimize time and extra cost due to repair these defects, the defective components must be identified at an early phase of the project. However, in current practice, inspecting defects is mostly manual interpretation of the geometric data at specific locations on the structure, which are acquired from measuring tapes, levelling or total stations. That leads to inspection results are subjective and insufficient to address detailed status of the structural components. Therefore, project managers cannot identify the defective components timely, accurately and objectively, and are difficult to integrate inspection results into digital tools to improve efficiency of the project management.

A terrestrial laser scanning can capture a highly detailed three-dimensional (3D) scene accurately and quickly, used at many construction sites in recent years. A point cloud is then processed for construction progress monitoring, as-built BIM, and quality control. For example, Turkan et al. (Turkan, 2014) proposed a method to monitoring construction progress based on secondary and temporary components in a construction site. from a 3D point cloud, but an accuracy can be improved by fusing additional information like color and 3D edge information. Additionally, recent effort in automatically extracting the structural components from the point cloud can be highlight by the work of Maalek et al. (Maalek et al., 2019) who introduce a planar segmentation based on linear features of the data points, a hierarchical clustering technique and context information of the structures to extract the floors, columns and rebars of reinforced concrete structures of regular rectangular buildings. In assessing dimensions of precast concrete elements, Kim et al. (Kim et al., 2016) used a principal component analysis to extract data points of surfaces, and edges and corners are subsequently extracted to determine the dimensions as well as to map to an as-design model for deviation assessment. Moreover, Wang et al. (Wang et al., 2017) proposed one-class support vector machine approach linearity, planarity and red-green-blue colors of the point cloud to extract individual rebars in concrete structures for quality assurance and control. Additionally, in practice, process pipelines based on commercial software (e.g. Revit, Autodesk Navisworks, Archicad) are still primarily manual through an interactive manner, in which users use as-built functions to process a point cloud, for example, segmentation and shape fitting. There work requires experienced users who can handle massive and complex data sets. Thus, efficient, automatic extraction of the structural components of the construction project is still high challenge.

To inspect the structures, Bosché and Guenet (Bosché and Guenet, 2014) mapped 3D point cloud to as-design BIM model and extracted a point cloud matching to a structural components in the BIM. Subsequently, Straightedge and F-Numbers were used to measure the deviation between the point cloud and BIM to identify a discrepancy between the as-design BIM and a

real construction for each floor. The authors also reported that this approach is given higher quality and much efficiency than that from the traditional methods. Moreover, Tang et al. (Tang et al., 2011) proposed three algorithms to inspect a floor defects through the surface flatness, which included range filtering, deviation filtering and sliding window, which a main difference between these methods is noise filtering algorithm. Principles of these methods is that after removing noise data of the surface, deviations between the points and the reference surface were computed to identify the surface flatness. Moreover, Truong-Hong and Lindenbergh (Truong-Hong and Lindenbergh, 2019) proposed point-surface, point-cell and cell-cell methods to measure deformation of the structure from a laser scanning data, which were then applied to estimate a vertical clearance of the bridge.

This paper proposes a new method to automatically extract point clouds describing floor and ceiling of the building. this work is done by using kernel density estimation (KDE) and a cell-based segmentation (CbS) to extract patches within 2D cells in the xy plane and to segment the patches belonging the surfaces of the floor and ceiling, respectively. Subsequently, point-surface (PS) and cell-surface (CS) methods are used to measure deformations of the floor and ceiling for identifying surface defects.

2. PROPOSED METHOD

In a construction project, when the storey is constructed completely, dimension quality control and surface defect detection of structural elements must be reported timely and accurately for decision making. A new storey can only start to construct when the report of quality control of constructed storey is approved. Moreover, an inspection often carries out for each storey separately, as such a point cloud captured in each story is used. As goal of this paper is to detect defects of floor/ceilings through deformation, the proposed method includes 2 Parts: (1) the floors/ceilings extraction and (ii) deformation measurement (Fig. 1). In *Part 1*, a 3D point cloud of a floor and ceiling are extracted from entire point cloud of a storey by using a combination between KDE (*Step 1*) and CbS method (*Step 2*), while in *Part 2*, PS and CS methods are used to determine vertical deformations of the floor/ceiling slabs.

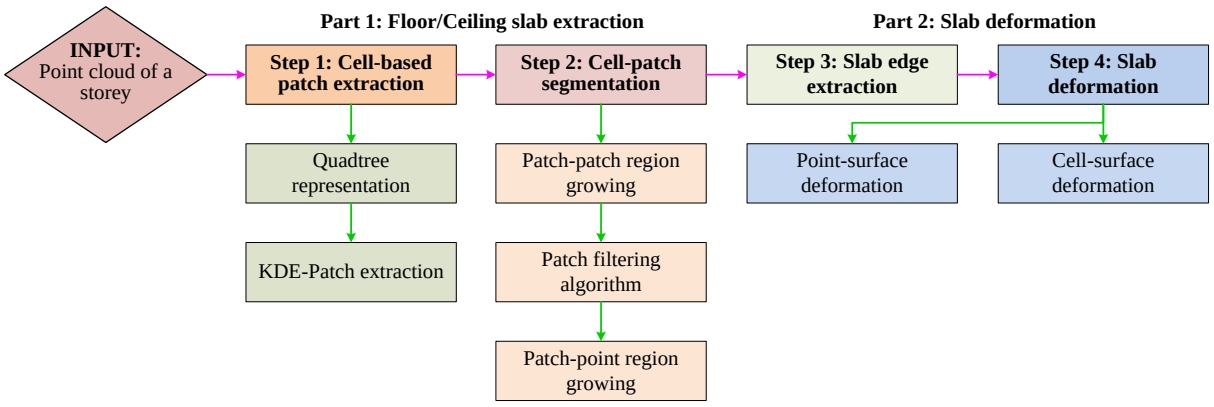

Figure 1. Proposed method for identifying surface defects of floor/ceiling slabs

Moreover, in reinforced concrete buildings, at the construction stage, floors/ceilings, or also called floor and ceiling slabs, appear as flat horizontal surfaces. The slab is a part of the floor/ceiling slabs supported by beams, columns and walls (Fig. 2).

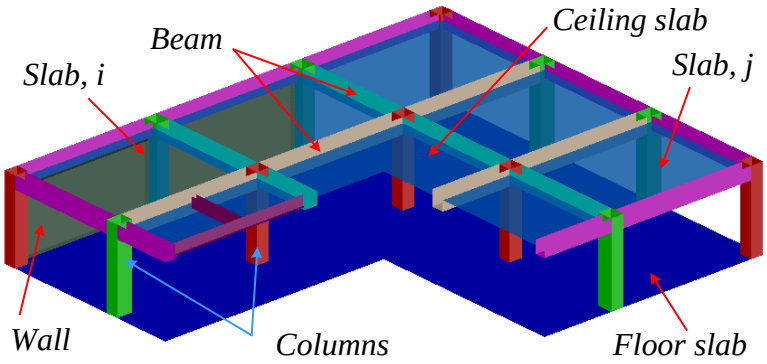

Figure 2. Structural elements in common reinforced concrete buildings

1.1 Part 1 - Floor/ceiling slab extraction

Step 1: **Cell-based patch extraction**

A point cloud ($\mathbf{P}_{storey} = (p_i \in R^3)$ of a storey building is decomposed into 2D cells ($\mathbf{C} = \{c_1, \ldots c_i, c_N\}$, i = [1, N]) by using a quadtree to recursively subdivide an initial minimum 2D bounding box of the points P_{st} along the x- and y- directions in a Cartesian coordinate system. Although many criteria are used to define a terminated subdivision conditions, the cell size is used in this study, which means the size of the cells on leaf nodes of the quadtree must be smaller than the cell size threshold. A selection of the cell size must be guarantee there is at least one cell can be represented the slab. Additionally, the cell is classified as "full" if it occupies a number of the points exceeding a predefined threshold called *min_ptc*; otherwise it is known as "empty". Thus, each cell c_i describes as a tuple (two opposite corners: [x_{min}, y_{min}; x_{max}, y_{max}]; classification: empty/full; points: $\mathbf{P}_{ci} = (p_{ci} = \{x_i, y_i, z_i) \mid \mathbf{P}_{ci} \in \mathbf{P}_{storey}\}$).

The 2D cell c_i may contain a point cloud of surfaces' patches ($\mathbf{\Psi} = \{\psi_{i1}, \psi_{ij}, \ldots, \psi_{in}\}$) of many structural components (e.g. floor, ceiling, beam or column) (Fig. 3a). Thus, the data points affiliated to a patch ψ_{ij} are extracted by KDE generated from the z-coordinate of the points (Laefer and Truong-Hong, 2017). As the patches of the slab's surface is often a horizontal plane and their locations are in separate positions in the vertical locations, the points belonging to the patch are located within two consecutive valleys of KDE (Fig. 3b), which can be expressed in Eq. 1

$$\psi_{ij} = (p_{\psi ij} \mid z_{valey,\,k} \le p_{\psi ij}.z \le z_{valey,k+1}) \qquad (1)$$

where $z_{valey,k}$ and $z_{valey,k+1}$ are coordinates of two consecutive valleys of the PDS.

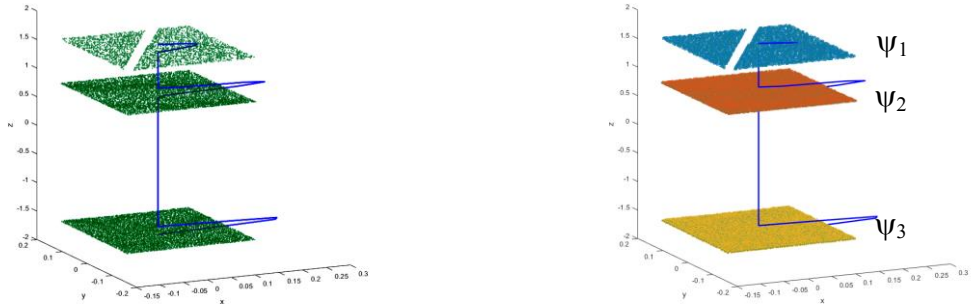

a) A point cloud and their distribution a long elevation

b) Extracting points presenting patches by using KDE

Figure 3. Extracting data points of patches within a 2D cell

Next, as the patch is assumed as a planar surface, a principal component analysis (PCA) is used to compute a normal vector of a fitting surface from a covariance matrix shown in Eq. 2 (Hoppe et al., 1992), while the centroid of the points $\mathbf{p}_{\psi ij}$ is considered as the point on the fitting surface (Eq. 3). Additionally, the root mean square distances from the points to a fitting plane defined, called a residual value (r_{ij}) is computed to measure variance of the points $\mathbf{p}_{\psi ij}$ to the fitting surfaces, given in Eq. 4 and 5. The patch ψ_{ij} describes as a tuple: $\psi_{ij}(p_{\psi ij.0}, n_{ij}, r_{ij})$,

$$\mathrm{cov}_{\psi ij} = \sum_{i=1}^{N}\left(p_{\psi ij} - p_{\psi ij.0}\right)\left(p_{\psi ij} - p_{\psi ij.0}\right)^{T} \quad (2)$$

$$p_{\psi ij.0} = \frac{1}{|P_{\psi ij}|}\sum_{i=1}^{N} p_{\psi ij} \quad (3)$$

$$r_{\psi ij} = \sqrt{\frac{1}{|d_{p\psi ij}|}\sum_{i=1}^{N} d_{p\psi ij}^{2}} \quad (4)$$

where $p_{\psi ij.0}$ is the centroid of the points $\mathbf{p}_{\psi ij} \in \psi_{ij}$ computed in Eq. 3, $|\ |$ is the cardinal of the $p_{\psi ij}$, and $d_{p\psi ij}$ is the distance from a point to $\psi_{ij}(p_{ij.0}, n_{ij})$, is given in Eq. 5.

$$d_{p\psi ij} = \frac{(x_i - x_0)n_{ij}.x + (y_i - y_0)n_{ij}.y + (z_i - z_0)n_{ij}.z}{\sqrt{n_{ij}^2.x + n_{ij}^2.y + n_{ij}^2.z}} \quad (5)$$

where x_0, y_0, z_0 are coordinates of $p_{\psi ij,0}$ while $n_{ij} = (n_{ij}.x, n_{ij}.y, n_{ij}.z)$ is the normal vector

Step 2: Cell-patch segmentation (CbG)

Goal of this step is to segments patches representing individual slabs of the floor and ceiling slabs. However, as one patch may contain points of multiple surfaces of structural elements (e.g. a slab, beam, column and/or wall), CbG consists of 3 sub-steps: patch-patch region growing (*Step 2.1*), forward and backward filtering (*Step 2.2*), and patch-point region growing (*Step 2.3*), as specified below.

Step 2.1: Patch-patch region growing

As a patch represents a local surface of a floor/ceiling surface, the patch-patch region growing is to segment the patches belonging to the same surface. The algorithm starts with an initial seeding patch ($\psi_{ij} \in c_i$) having the smallest residual value ($min\_r_{\psi ij}$) and then the neighbouring patches ($\psi_{kj} \in c_k$) are retrieved, in which the cell c_k is adjoined to the cell c_i. The patch ψ_{kj} can be added to a region (R_k) of the patch ψ_{ij} if Eq. 6 is satisfied. Once the patch ψ_{kj} adding to the region R_k, if the residual ($r_{\psi kj}$) of the patch is smaller than a predefined residual threshold (r_0), the patch is added to the seeding patch set. The algorithm is iteratively checked the patches and generates a set of the regions $\mathbf{R} = \{R_1, \ldots, R_k, R_N \mid R_k = (\psi_{ij})\}$ containing the patches. The growing process is completed when the predefined patches are checked. For details of the patch-patch region growing can refer to (Rabbani et al., 2006; Truong-Hong et al., 2018).

$$\begin{cases} \angle n_{ij}, n_{kj} \leq \alpha_0 \\ d\left(p_{\psi kj,0}, \psi_{ij}\right) \leq d_0 \end{cases} \quad (6)$$

where $\angle n_{ij}, n_{kj}$ is a deviation of the normal vectors, $d\left(p_{\psi kj,0}, \psi_{ij}\right)$ is the distances from the centres of ψ_{kj} to the patch ψ_{ij}, and α_0 and d_0 are respectively a predefined angle and distance threshold.

Once the patch contain the point cloud of the slab, column, beams and/or wall, there are two cases can occur: (1) the patches is segmented but it contains the data points of other structural components, and (2) the patch does not segment because the patch's features differ from ones of the slab's patches. That can be solved in *Step 2.2* and *Step 2.3*, respectively.

Step 2.2: *Patch filtering algorithm*

Since the patches contains the points of other structural components often locate on a boundary of a region, the algorithm classified the patches $\psi_{ij} \in R_k$ into boundary and interior patches ($\psi_{ij.bound}$ and $\psi_{ij.interior}$). The patch is the boundary patch if the cell occupying this patch connects to less than 8 other cells occupying other patches of the region R_k, otherwise it is the interior patch (Fig. 4a). Additionally, from the boundary patch $\psi_{ij.bound} \in R_k$, the interior patches $\psi_{kj.interior}$, which the neighbour patches of $\psi_{ij.bound}$, are extracted, and then a local surface ψ_{Rkj} of the region R_k is estimated from the points belonging to $\psi_{kj.interior}$ using Eq. 2 and 3. Subsequently, the points $p_{\psi ij} \in \psi_{ij,bound}$ are considered as inlier points $p_{\psi ij,inlier}$ if the distance from the points to the local surface ψ_{Rkj} is no larger than the distance threshold d_0, as given in Eq. 7 (Fig. 4b). The outlier points are then eliminated out of the patch.

$$p_{\psi ij} \rightarrow p_{\psi ij.inlier} \; if \; d\left(p_{\psi ij}, \psi_R\right) \leq d_0 \quad (7)$$

where $d\left(p_{\psi ij}, \psi_R\right)$ is the distance from the points $p_{\psi ij}$ to the surface ψ_R and d_0 is the distance threshold

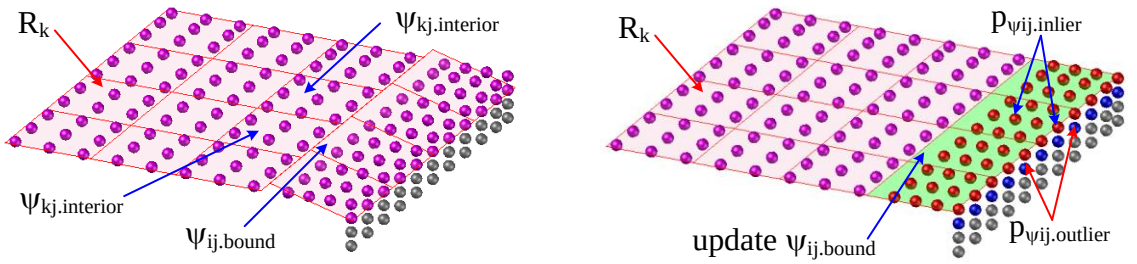

a) Point cloud in the boundary patch before filtering

b) Point cloud in the boundary patch after filtering

Figure 4. Illustration of patch filtering algorithm

Step 2.3: *Patch-point region growing*

Step 2.3 is aimed to extract the points of the slab, which are occupied by an unsegmented patch or the patches belonging to adjacent segments. The process starts with the boundary patch $\psi_{ij,bound} \in c_i$ of the region R_k to search adjacent patches ψ_{lm} occupied by an adjacent cell c_l of the cell c_i, where the patches ψ_{lm} do belong to the region R_l (Fig. 5a). Notably, the cells are considered as the adjacent cells if they share an edge and. Next, the points $\mathbf{p}_{\psi lm.Rk} \subset \mathbf{p}_{\psi lm}$ are added to the region R_k if the distance from the points $\mathbf{p}_{\psi lm.Rk}$ to the fitting surface of the patch $\psi_{ij,bound}$ satisfies Eq. 7 (Fig. 5b). Subsequently, if the percentage of points $\mathbf{p}_{\psi lm.Rk}$ to be added to R_k is empirically more than 50% of $|\mathbf{p}_{\psi lm}|$, the patch ψ_{lm} considered as a new boundary patch of the region R_k. Patch-point region growing iteratively re-gains points of the region R_k locating in adjacent patched, until no more point is added.

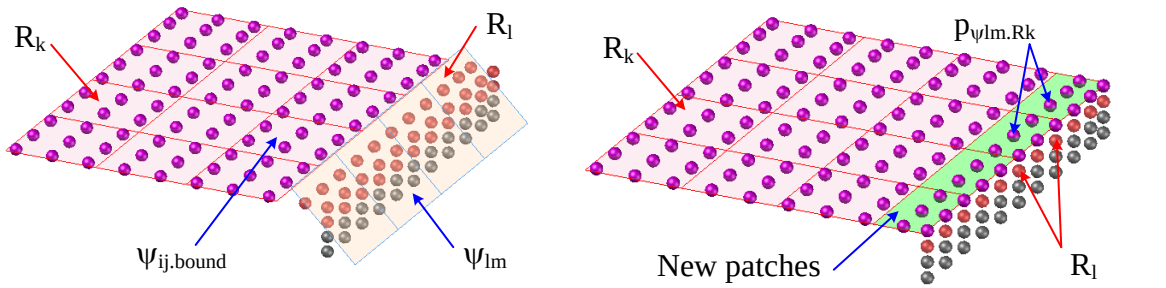

a) Points in a region before patch-points region growing

b) Points in a region after patch-points region growing

Figure 5. illustration of patch-points region growing

1.2 Part 2: Slab deformation

In reinforced concrete buildings, slabs are often supported by beams columns, and/or walls. Edges of the slab, where is an intersection between the slab's surface and surfaces of supported elements (S_{SE}), are considered as fixed, which implied there is no deformation at these locations. In this study, deformation of the slab supported by the beams and/or walls are

computed, but it can be simply extended for other types of the slabs because they are based on the same hypothesis.

Step 3: Slab edge extraction

Due to an edge loss during data acquisition or segmentation and complexity of the scene itself (Tang et al., 2009), a gap between the slab and S_{SE} (e.g. beams and walls) are often available. The points on a boundary of the slab may not fully represent the slab edge because the edge loss or missing data. Moreover, the points of S_{SE} locate close to the slab edges.

As such, from the boundary patch $\psi_{ij.bound}(p_{\psi ij.0}, n_{ij}) \in c_i$ of the slab $R_k \equiv S_k$, the points $\mathbf{P}_{vicinity}$ within the cell c_i and adjoined cells c_j of the cell c_i are extracted (Fi.g 6a). Notably, the adjoined cell c_j is the cells sharing edges to the cell c_i and do not occupy the patches belonging to the slab S_k. Moreover, the points $p_{\psi ij} \in \psi_{ij,bound}$ are also eliminated out of the points $\mathbf{P}_{vicinity}$. Subsequently, the candidate points ($\mathbf{P}_{SE.candidate}$) of S_{SE} are then roughly extracted, which is the points having the distance to the fitting surface $\psi_{ij.bound}(p_{\psi ij.0}, n_{\psi ij})$ less than a predefined threshold d_1 (Fig. 6b). In this study, the threshold d_1 = 0.3m is selected, which can be the smallest height of the beams.

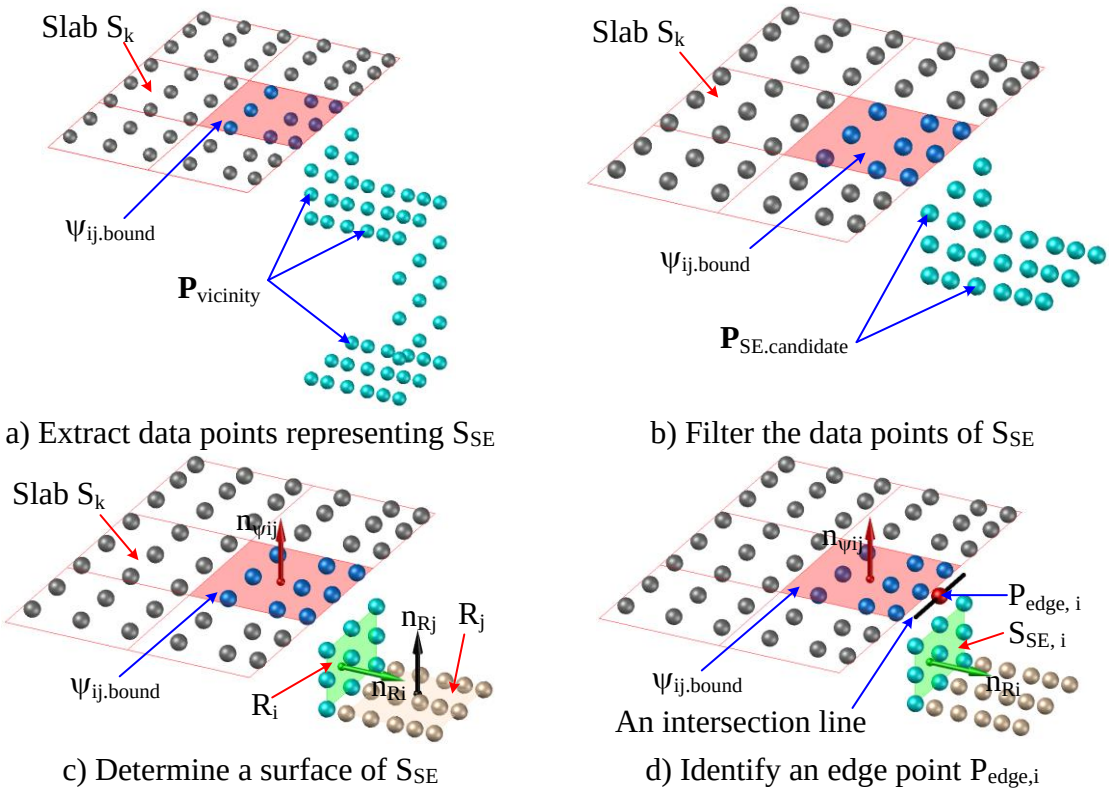

a) Extract data points representing S_{SE} b) Filter the data points of S_{SE}

c) Determine a surface of S_{SE} d) Identify an edge point $P_{edge,i}$

Figure 6. Illustration of the slab edge determination

In addition, a region growing is employed to segment the points $\mathbf{P}_{support.candidate}$ (Rabbani et al., 2006). Resulted segmentation are given several regions $\mathbf{R}$ = (R_1, R_2, ..., R_i, R_N), and then a

fitting surface of each region can be estimated based on Eq. 2 and 3 (Fig. 8c). Moreover, based on observation of the building structure, S_{SE} is close and perpendicular to the slab. Thus, the correct S_{SE} is the region satisfies conditions in Eq. 8. Finally, an intersection line between the boundary patch $\psi_{ij.bound}$ and the $S_{SE,i}$ is determined and the point $P_{edge,i}$ at the middle of the line segment of the intersection line is used as the point represent the slab edge segment (Fig. 8d).

$$R_i \rightarrow S_{SE,i}\ if\ \begin{cases} \cos\left(n_{\psi ij}, n_{Ri}\right) \leq \cos\left(\frac{\pi}{2} - \alpha_0\right) \\ d\left(p_{\psi ij.0}, p'_{Ri.0}\right) \rightarrow min \end{cases} \quad (8)$$

where $n_{\psi ij}\ and\ n_{Ri}$ are normal vectors of the fitting surfaces of the boundary patch $\psi_{ij.bound}$ and the region R_i, $p'_{Ri.0}$ is a projection of the centroid of the points belonging to the region R_i, and α_0 is the predefined angle threshold.

Step 4: Slab deformation

As mentioned above, the slab edges are fixed. The fitting surface through the edge points $P_{edge,i}$ is estimated and considered as the reference surface (S_{ref}), which is done by using Eq. 2 and 3. Next, the point-surface method is used to determine the slab deformation, in which the deformation is the distance from the points to the reference surface.

However, during data acquisition and registration, and floor/ceiling slab extraction, errors are inevitable. To reduce a negative impact of such errors to determine the slab deformation, the cell-surface method is employed to compute the slab deformation. In this method, the point cloud of the slab is decomposed into 2D cells in the xy plane, which is done similar to *Step 1.1*. For each cell, the centroid ($p_{ci,0}$) of the points within the cell is determined based on Eq. 3, which is represent to the cell. Subsequently, the distance from the point $p_{ci,0}$ to the reference surface S_{ref} is known as the slab deformation. More details of both point-surface and cell-surface methods can refer to Truong-Hong and Lindebergh (Truong-Hong and Lindenbergh, 2019).

3. EXPERIEMENTAL TEST, RESULTS AND DISCUSSION

To demonstrate the proposed method, a ground storey of a office building on Pham Ngu lao st in Ho Chi Minh city, Vietnam is selected. The storey is about 18.5m wide x 29.5m long x 3.45m high. Structural elements consist of floors connected to a basedment, ceilings, columns, beams (primary and secondary) and walls. The building storey was scanned by a Trimble TX8 with a maximum scanning range at 120m and an angular accuracy of 8μrad in both vertical and horizontal (Trimble, 2020b). During data acquisition, a point spacing of 11.3mm at a range of 30m was used. A total of 11 scanning stations was established to maximize data coverage of an interior storey (Fig. 7). The point clouds of scanning stations were registered by the Trimble RealWork software v11.2 (Trimble, 2020a) and the registration error was about 1.57mm based on cloud-cloud registration. Finally, 23.9 million points of the building storey was exported with x-, y- and z- coordinates for each point as input data for the proposed method. Notably, parts of a MEP system were installed, which obstructs to capture surfaces of the structural element.

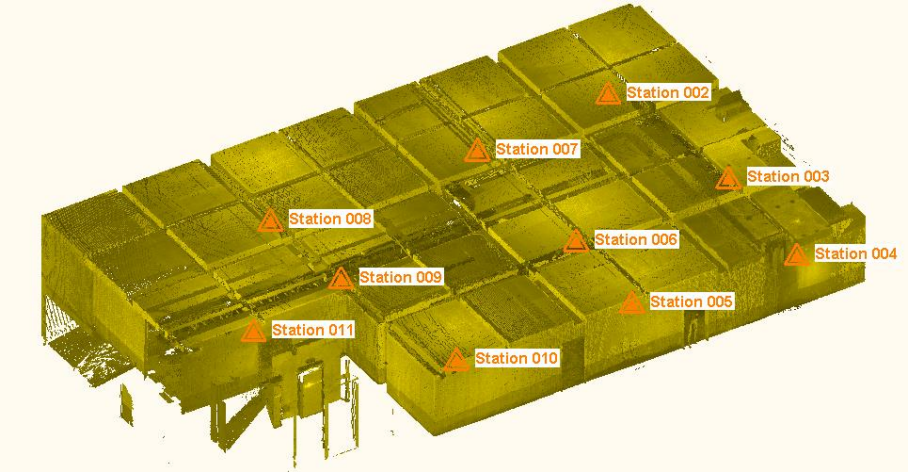

Figure 7. Point cloud of a storey from an internal scan

The quadtree is used to generate 2D cells in a xy plane from the point cloud of the storey, in which the cell size of 1.0m is used as a termining subdivision condition and while the number of points, *min_ptc* = 10 is used for classifying the cell as "*empty*" or "*full*" (Fig. 8a). To ensure the slab can be segmented based on pacthe-patch region growing (*Step 2.1*), this requires at least one patch (or cell) representing the slab that is to be an initial seeding patch in *Step 2.1*. As such, this selected cell size is corresponding to the smallest surface of the slab by 2mx2m. Moreover, to distinguish data points of an individual patch within the cell in an elevation direction, the bandwidth for KDE must be smaller than the distance between two consecutive surfaces in the elevation direction. As such, the bandwidth of 0.2m is selected, which is the smallest thickness of the structural components. The patches in the cell is ordered in the z coordinate of the patch center, which implies the first patch is the lowest one. Results of 2D cell decomposition and patches within the cells are shown in Fig. 8.

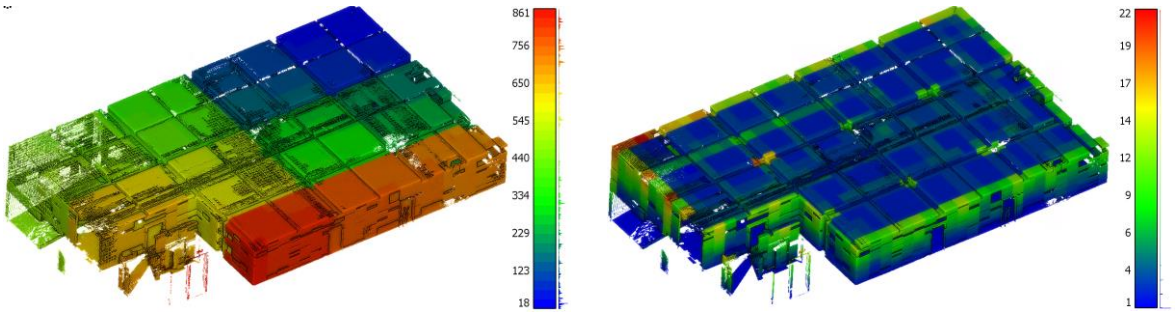

a) 2D cells rendering according to cell indices

b) 2D cells rendering according to patch indices

Figure 8. 2D cell decomposition and patches within the cells

Next, CbG is used to extract the floor and ceiling slabs. This method requires the angle threshold α_0, the distance threshold d_0 and the residual threshold r_0. As concrete floor and ceiling slabs

are mostly smooth, horizontal, flat surfaces, the values of these thresholds: $\alpha_0 = 5$ degrees, $d_0 = 10$mm and $r_0 = 10$mm are selected. Notably, although the surfaces of the supported structural elements (e.g. columns, beams, walls) are perpendicular to the slab's surface, the small value of α_0 is selected to prevent the segmentation including the points of the MEP components, while both the distance and residual values are to compensate a data error, and there values must be adjusted based on the data errors or the surface roughness.

Additionally, the patches of the surfaces belonging to the floor and ceiling are mostly the first and last patches of a cell in the vertical direction, respectively. Therefore, for floor extraction, only the first patches $\psi_{i1} \in c_i$ are used as an input data in *Step 2.1* and *2.2* instead of all patches, while for the ceiling, the last patches $\psi_{iN} \in c_i$ are used as an input data in *Step 2.1* and *2.2*. Moreover, in *Step 2.3* all remaining patches in the cells are used. Notably, when the patches are assigned as the floor and/or ceiling, they are immediately deactivated. Results of the segmentation of the floor and ceiling slabs are shown in Fig. 9. It is successful in extracting all surfaces of the floor and ceiling slabs.

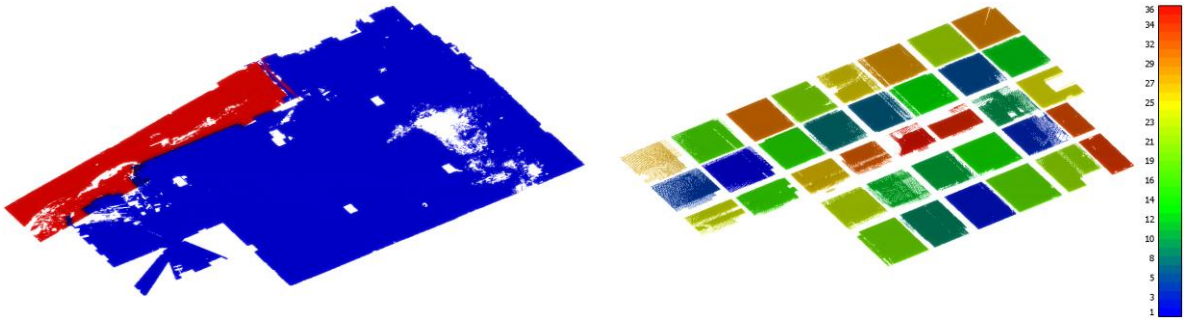

a) Results of the floor slab b) Results of the ceiling slab

Figure 9. Extraction of the floor and ceiling slabs by using cell-patch segmentation

As the deformation of the floor of the storey was reported when completing a construction of the basement storey, in this study, only deformations of the ceiling slabs are measured. Additionally, in this case, the slab is supported by beams and walls, and the slabs of the ceiling are separately. As due to occlusion, parts of surfaces of the beams and walls supported the slab cannot be extracted (Fig. 9a). Based on the slab edge computed in *Step 3*, deformations of individual slab are computed through PS and CS methods (Fig. 9b-f). Notably, the deformations here are relative deformation respecting to the edge of the slab, which is assumed no deformation. Moreover, to investigate influence of the cell sizes on deformations derived from CS method, the cell size varied in a range from 50mm to 200mm with an interval of 50mm are used.

The slab deformations vary in a range from -36.04mm to 42.03mm from PS method and -24.10mm to 36.84mm for CS method with the cell size of 150mm and 200mm (Table 1). It finds that a large positive value of the deformations occurs around the lift where the point cloud of the lift's wall above the slab does not fully eliminate out of the slab segment. However, means of the deformation is in a range from -1.47mm to -1.65mm for both methods.

Interestingly, approximately 75% of the points has the deformations varying in a range a mean deformation ± a standard deviation (Table 1). Additionally, by using different cell sizes in CS method, the deformations vary in a small range. However, when the cell size is small and the number of the points within the cell is smaller than a predefined value, 5 points required in this study, parts of the slab are missing results (Figure 9c and d). As such, the selection of the cell size value must be based on the point spacing. Finally, although the proposed method is used for computing the slab deformation supported by the beams and/or walls, it can simply extended for other types of the slabs, in which the approach to determine the slab's edge points must be adapted for other types of the slabs.

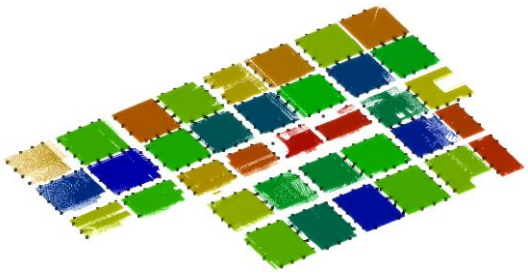

a) Edge points (black dots) and point cloud of the slabs

b) Deformations derived from PS method

c) Deformations derived from CS method with the cell-size of 50mm

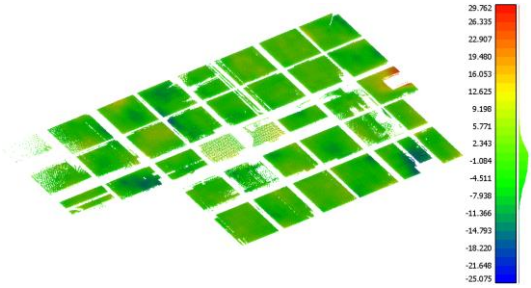

d) Deformations derived from CS method with the cell-size of 100mm

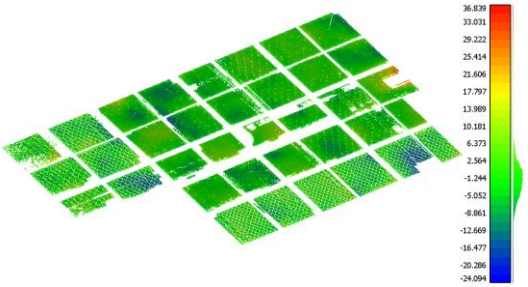

e) Deformations derived from CS method with the cell-size of 150mm

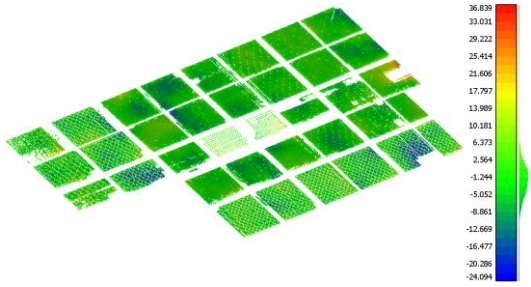

f) Deformations derived from CS method with the cell-size of 200mm

Note: negative values show the slab sagging while positive values is for hogging

Figure 10. Deformation of the slabs of the ceiling (Unit: mm)

Table 1. Summarized deformations of the slabs

Aspect	PS method	CS method with various cell size			
		50mm	100mm	150mm	200mm

Minimum (mm)	-36.04	-24.71	-25.08	-24.10	-24.10
Mean (mm)	-1.54	-1.50	-1.65	-1.47	-1.64
Standard deviation (mm)	4.03	4.33	4.39	4.51	4.44
Maximum (mm)	42.03	26.71	29.76	36.84	36.84
Percentage of points in a range [Mean ± Std]	73.8%	73.2%	74.2%	74.1%	74.6%

Finally, the proposed method is implemented in MATLAB 2019b (MathWorks, 2019b), and 23.9 million data points of a building storey is processed Dell Precision Workstation with a main system configuration as follows: Intel(R) Xeon(R) W-2123 CPU @ 3.6GHz with 32GB RAM. The processing time is 78.9 seconds including executing time for quadtree decomposition about 24.7 seconds, extracting patches within the cells about 19.2 seconds, for extracting points of the floor and ceiling about 19.7 seconds and 16.1 seconds, respectively. That implies the proposed method is efficiency to handle a large data set from a construction project.

4. CONCLUSIONS

The paper presents an efficient, automatic method to extract floor and ceiling slabs of a reinforced concrete building for inspecting defects through deformation. The proposed method decomposes the point cloud of the building into 2D cells in xy plane and a synergy between KDE and CbS is used to extract point clouds belonging to surfaces of the floor and ceiling. Subsequently, surfaces of beams and walls supported the slabs are extracted to determine the slab edges, where are considered as no deformation. An experimental test on 23.9 million points of the building shows the proposed method extracts the surfaces of floor and ceiling successfully and efficiently, in which executing time for the floor and ceiling extraction is about 78.9seconds. Additionally, both PS and CS methods are can report detailed deformations of the slab, which can be used for other similar structures. Interestingly, the selection of the cell size in CS method must ensure the cell occupied sufficient number of the points, otherwise, the deformation-based CS method may not available in parts of the slab where the point spacing is larger than the cell size. Although the proposed method is developed for inspecting deformations of the slabs supported by the beams and walls, which is a popular slab in the building structures, the method can be easily extended for other types of the slab. Moreover, in future work, the proposed method will extent to extract other structural elements (e.g. columns, beams and walls) for dimensional quality, surface defects, as well as as-built model reconstruction.

ACKNOWLEDGEMENT

This work was funded by the generous support of the European Commission through H2020 MSCA-IF, "*BridgeScan: Laser Scanning for Automatic Bridge Assessment*", Grant 799149. The first author is graceful for this support. The authors also thank Dat Hop Company Limited and Ceotic., JSC for their providing the laser scanning data.

BIOGRAPHICAL NOTES

Dr. Linh Truong-Hong is a Marie Curie Fellowship at Optical and Close Laser Scanning Group, Department of Geoscience and Remote Sensing, TUDelft. His research interests are to develop an integrated framework to deploy laser scanning and photogrammetry for civil infrastructure inspection and monitoring, construction management and urban modelling. He has published more than 50 scientific papers, which include 3 book chapters, 22 journal peer review papers and 30 conference papers, and filed 2 patents. His publications have more than 797 citations resulting in an H-index of 15 according to Google Scholar. Moreover, his research activities were recognized through 7 prizes and award, which includes 2019 Mandy Prize ICT/GIS/BIM by Institute Civil Engineering, the best paper at CERI 2018, 2015 IQPC Best track ward awarded by ISPRS, First place 2015 IEEE GRSS Data Fusion Contest, Highly Recommended Award, the 13th International Conference on Computational Science and Applications (ICCSA) 2013.

CONTACTS

Dr. Linh Truong-Hong
Department of geoscience and Remote Sensing, Delft University of Technology
Address: Room 2.28, Building 23, Steviweg 1/PO box 5048, 2628 CN Delft Delft
THE NETHERLANDS
Tel. + 31 15 27 88147
Email: l.truong@tudelft.nl
Web site: https://www.tudelft.nl/en/ceg/about-faculty/departments/geoscience-remote-sensing/staff/researchers/dr-l-linh-truong-hong/

REFERENCES

Bosché, F., Guenet, E., 2014. Automating surface flatness control using terrestrial laser scanning and building information models. *Automation in Construction* 44, 212-226.

Hoppe, H., DeRose, T., Duchamp, T., McDonald, J., Stuetzle, W., 1992. Surface reconstruction from unorganized points, ACM SIGGRAPH 1992, Chicago, USA, pp. 71-78.

Kim, M.-K., McGovern, S., Belsky, M., Middleton, C., Brilakis, I., 2016. A suitability analysis of precast components for standardized bridge construction in the United Kingdom. *Procedia engineering* 164, 188-195.

Laefer, D.F., Truong-Hong, L., 2017. Toward automatic generation of 3D steel structures for building information modelling. *Automation in Construction* 74, 66-77.

Love Peter, E.D., 2002. Influence of Project Type and Procurement Method on Rework Costs in Building Construction Projects. *J. Constr. Eng. M.* 128, 18-29.

Maalek, R., Lichti, D.D., Ruwanpura, J.Y., 2019. Automatic recognition of common structural elements from point clouds for automated progress monitoring and dimensional quality control in reinforced concrete construction. *Remote Sensing* 11, 1102.

MathWorks, 2019b. MATLAB Function Reference., 2019b ed.

Rabbani, T., Heuvel, F.v.d., Vosselmann, G., 2006. Segmentation of point clouds using smoothness constraint. *International Archives of Photogrammetry, Remote Sensing and Spatial Information Sciences* 36, 248-253.

Tang, P., Akinci, B., Huber, D., 2009. Quantification of edge loss of laser scanned data at spatial discontinuities. *Automation in Construction* 18, 1070-1083.

Tang, P., Huber, D., Akinci, B., 2011. Characterization of Laser Scanners and Algorithms for Detecting Flatness Defects on Concrete Surfaces. *Journal of Computing in Civil Engineering* 25, 31-42.

Trimble, 2020a. Trimble RealWorks v11.2. *Trimble*.

Trimble, 2020b. Trimble TX8 LASER SCANNER. *Trimble*.

Truong-Hong, L., Chen, S., Cao, V.L., Laefer, D.F., 2018. Automatic Bridge Deck Damage Using Low Cost UAV-based Images.

Truong-Hong, L., Lindenbergh, R., 2019. Measuring deformation of bridge structures using laser scanning data, 4th Joint International Symposium on Deformation Monitoring (JISDM), Athens, Greece, p. 7.

Turkan, Y., 2014. Tracking of secondary and temporary objects in structural concrete work. *Construction Innovation* 14, 145-167.

Wang, Q., Cheng, J.C.P., Sohn, H., 2017. Automated Estimation of Reinforced Precast Concrete Rebar Positions Using Colored Laser Scan Data. *Computer-Aided Civil and Infrastructure Engineering* 32, 787-802.